


Article

Explosion Load Characteristics of Fuel—Air Mixture in a Vented Chamber: Analysis and New Insights

Xingxing Liang¹, Yaling Liao¹, Zhongqi Wang², Huaming An^{1,3,*}, Junjie Cheng¹, Chunliu Lu¹
and Huajiao Zeng¹

- ¹ Faculty of Public Security and Emergency Management, Kunming University of Science and Technology, Kunming 650500, China; xingxingliang@kust.edu.cn (X.L.); liaoyaling@stu.kust.edu.cn (Y.L.); chengjunjie@stu.kust.edu.cn (J.C.); luchunliu@stu.kust.edu.cn (C.L.); huajiaozeng@stu.kust.edu.cn (H.Z.)
- ² State Key Laboratory of Explosion Science and Safety Protection, Beijing Institute of Technology, Beijing 100081, China; czqwang@bit.edu.cn
- ³ Geotechnical Institute, TU Bergakademie Freiberg, 09599 Freiberg, Germany
- * Correspondence: huaming.an@kust.edu.cn

Abstract: The advances in research on the explosion load characteristics of the fuel–air mixture in vented chambers are reviewed herein. The vented explosion loads are classified into three typical types based on this comprehensive literature research. These models are the accumulation load model, attenuation load model, and interval jump load model. The characteristics of the three different typical vented explosion load models are analyzed using Fluidy-Ventex. The research results show that overpressure is largely determined by methane concentrations and vented pressure. The turbulent strength increased from the original 0.0001 J/kg to 1.73 J/kg, which was an increase of 17,300 times, after venting in the case of a 10.5 v/v methane concentration and 0.3 kPa vented pressure. When the vented pressure increased to 7.3 kPa, the turbulent strength increased to 62.2 J/kg, and the overpressure peak correspondingly increased from 69 kPa to 125 kPa. In the case of the interval jump load model, the explosion overpressure peak tends to ascend when the intensity of the fluid disturbance rises due to the venting pressure increasing at a constant initial gas concentration. When the venting pressure reaches tens of kPa, the pressure differential increases sharply on both sides of the relief port, and a large amount of combustible gas is released. Therefore, there is an insufficient amount of indoor combustible gas, severe combustion is difficult to maintain, and the explosion load mode becomes the attenuation load model.



Citation: Liang, X.; Liao, Y.; Wang, Z.; An, H.; Cheng, J.; Lu, C.; Zeng, H. Explosion Load Characteristics of Fuel—Air Mixture in a Vented Chamber: Analysis and New Insights. *Energies* **2024**, *17*, 5649. <https://doi.org/10.3390/en17225649>

Received: 8 October 2024
Revised: 7 November 2024
Accepted: 9 November 2024
Published: 12 November 2024



Copyright: © 2024 by the authors. Licensee MDPI, Basel, Switzerland. This article is an open access article distributed under the terms and conditions of the Creative Commons Attribution (CC BY) license (<https://creativecommons.org/licenses/by/4.0/>).

Keywords: gas explosion; vented explosion; blast load models; numerical simulation

1. Introduction

Gas explosions have been proven to cause significant damage to buildings. Predicting gas explosion loads reasonably and effectively is an important part of the design of blast-resistant structures. Researchers have been developing methods for predicting gas explosion loads for a long time. Many methods have been established to calculate the blast loading in a condensed-phase explosive in UFC 3-340-02 [1]. Therefore, equivalent TNT charge is a widely used method in practice. In addition, the Strehlow curves and the multi-energy method obtain the blast loading based on the flame spreading speed or blast strength in the TNO Yellow Book [2]. However, this is not the case when a gas explosion occurs in a vented chamber. Doors and windows will become pressure relief channels during the blast of the gas explosion process in a vented chamber. Explosion venting is one of the effective methods to reduce gas explosion disasters. However, unreasonable venting may trigger secondary disasters, such as external explosions and indoor secondary explosions.

In this paper, we present a review of and some new insights into the explosion load characteristics of the fuel–air mixture in a vented chamber. Firstly, in Section 2, the advances in the research on the explosion load characteristics of the fuel–air mixture in a vented

chamber are discussed, and vented explosion loads are classified into three typical types based on this comprehensive literature research. The theory of numerical modeling of vented explosion load models is presented in Section 3, and then, the three typical vented explosion loads simulation is conducted in Section 4, where the mechanisms of producing significant pressure during vented explosions are discussed. Finally, some conclusions are drawn in Section 5. It should be pointed out that the present review and study only focus on a methane–air mixture explosion in an empty vented chamber. The obstacle problems of chamber are not covered.

2. Advances in the Research on the Explosion Load Characteristics of the Fuel–Air Mixture in a Vented Chamber

The causes of load formation during a gas explosion and venting process are complex, drawing the research interest of a number of outstanding scholars over the past 40 years. Below, we provide a review from three aspects: explosion pressure and influencing factors, flame characteristics and stability research, and numerical simulation and experimental research on venting explosions.

2.1. Explosion Pressure and Influencing Factors

Explosion pressure refers to the instantaneous pressure generated during an explosion, which is influenced by various factors including fuel type, container structure, ignition location, and vent size. In recent years, increasing attention has been paid to how these factors affect the variance in explosion pressure, providing guidance for safety design and risk assessment. Therefore, the following review summarizes the research on explosion pressure and its influencing factors, aiming to provide a comprehensive perspective on this complex phenomenon.

Cooper et al. [3] proposed that four distinct pressure peaks exist within a container, corresponding to different combustion steps, including vent failure, external explosions, maximum flame area, and oscillatory peak. Additionally, Harrison et al. [4] noted that external pressure peaks are primarily caused by external fuel–air explosions rather than internal factors. Bauwens et al. [5] experimentally studied the effects of ignition location, vent size, and obstacles on explosion development, proposing a simple model to estimate the maximum pressure of major transient pressures. Chao J et al. [6] further explored the impact of fuel, confined space size, and ignition position on pressure development, finding interactions between peak pressure, maximum flame area, combustion velocity, and overpressure generated by external explosions. Taveau et al. [7] performed an experimental study on vented gas explosions and vented dust explosions. They highlighted the key detection of such studies, identified the conditions under which secondary explosions occur, and compared the experimental data with standard applications to propose elements for selecting more appropriate correlations.

Fakandu et al. [8] researched dynamic rupture pressure, discovering that it exceeds static rupture pressure, and proposed a proportional constant.

In addition, Molkov et al. [9] improved the predictive capability of vent size correlations, emphasizing the relationship between dimensionless deflagration overpressure and turbulent Bradley number. Jin Guo et al. [10] studied the vent rupture pressure of methane–air mixtures in small cylindrical containers, noting that Helmholtz oscillations could still occur even when vent areas were much smaller than previously studied. Furthermore, Shao Hao et al. [11] investigated the explosive venting characteristics of coalbed methane transfer pipelines, proposing a venting scheme to mitigate external environmental impacts. Makarov et al. [12] introduced an engineering correlation considering various influencing factors of local vented deflagration overpressure, including turbulence generated by the flame front and the flow state of the initial mixture. Minggao YU et al. [13] concluded a small-scale simulated pipeline experiment and showed that the development of overpressure affected by the side vent is influenced by both the location of the side vent and the interaction between the side vent and the end vent. Chuanyu Pan et al. [14]

indicated that circular and square explosion vents have almost the same venting effect through experiments. Changshuai Zhang et al. [15] found that increasing the number of venting ports plays a minor role in increasing venting efficiency when the total venting port area is the same. Su Zhang et al. [16] concluded, through detonation experiments, that increased panel density raises maximum approximate overpressure, while panel inertia does not affect the second and third pressure peaks. Lastly, Qiang Zhang et al. [17] established a correlation between maximum overpressure and venting coefficient, revealing the Helmholtz oscillation phenomenon and the evolution of the flame front. Zhou Y et al. [18] studied the effects of ignition height on overpressure in hydrogen clouds, exploring the mechanisms of buoyancy effects and pressure wave interaction. Qi B et al. [19] numerically studied the propagation of a premixed flame in a pipe with a lateral vent, revealing the influence of the position and size of the lateral vent on the flame behavior and the internal mechanism of venting explosion. Recent research by An and Mu et al. [20] on rock fracture induced by high ground stress in deep mining highlights the importance of understanding pressure dynamics in geological contexts. Their findings suggest that the mechanisms of rock failure under high-stress conditions can parallel the understanding of pressure fluctuations in explosive environments.

In summary, explosion pressure is influenced by multiple factors, and researchers continually deepen their understanding of this phenomenon through experiments and theoretical models. Therefore, future research could further explore the relationships between pressure dynamics and flame behavior under varying conditions, providing more detailed foundations for enhancing safety and scientifically managing explosion risks. These studies hold significant importance not only for industrial safety but also for providing a basis for scientific inquiry in related fields.

2.2. Flame Characteristics and Stability Research: Key Factors in Explosion Safety

The study of flame characteristics and stability is a crucial field in understanding gas explosions and combustion, involving various factors such as fuel type, ventilation conditions, and environmental pressure. In recent years, advancements in experimental and numerical simulation techniques have led to a deeper understanding of flame dynamics, turbulence characteristics, and the interaction between flames and structures. This sub-section summarizes the relevant research, focusing on the factors influencing flame characteristics and stability under different conditions, providing essential insights for preventing explosion incidents and optimizing safety designs.

Shearer et al. [21] indicated that, when the duration of vented explosion loads is comparable to the resonance period of a structure, significant dynamic responses can lead to effective loads exceeding static loads. This finding establishes a theoretical basis for evaluating structural performance during explosion events. Molkov et al. [22] obtained typical turbulence factors and deflagration–outflow interaction numerics for vented explosions at initial pressures above atmospheric pressure through experiments, further revealing the complexities of flame propagation under high-pressure conditions. Razus et al. [23] provided a comprehensive review of various computational methods, elucidating their effective ranges and physical backgrounds, which serves as guidance for subsequent studies. Molkov et al. [24] studied the complex and simultaneous interactions between internal and external deflagrations in a SOLVEX confined atmospheric system through a combined experimental and theoretical approach.

Makarov et al. [25] developed a large eddy simulation (LES) model to simulate hydrogen–air explosions released through pipelines, introducing subgrid scale flame wrinkling factors to capture the primary phenomena in vented deflagrations. Subsequently, Bauwens et al. [26] combined experimental and numerical simulations to investigate methane–air deflagrations in vented enclosed spaces using an LES solver developed with the OpenFOAM CFD toolbox, exploring the impacts of subgrid turbulence and flame wrinkling. Makarov et al. [27] conducted benchmark experiments comparing the performance

of computational fluid dynamics (CFD) models in predicting deflagrations of homogeneous fuel–air mixtures and concentration gradient mixtures.

Ruipengyu Li et al. [28] performed numerical studies on fuel–air deflagration based on large eddy simulation (LES). They indicated that the time and amplitude of the peak overpressure strongly depend on the level of flame/turbulence interaction, which is determined by the number and location of obstacles. Furkan Kodakoglu et al. [29] conducted a rich fuel mixture explosion experiment and found that a flashback phenomenon was observed after an external explosion. Toliás et al. [30] performed numerical studies on fuel–air deflagration in actual scale vented rooms, focusing on two empirical parameters: turbulence flame speed based on modified Yakhot equations and Rayleigh–Taylor instability. Xing Huadao et al. [31] experimentally investigated the effects of ignition location and vent area on the explosion characteristics of a 9.5 vol% methane–air mixture, analyzing the influences of hydrodynamic instability, diffusion-thermal instability, and R–T (Rayleigh–Taylor) instability on the flame front. Sun et al. [32] observed and analyzed flame morphology in experiments and simulations, capturing trends in propagation characteristics across different stages. SU Bin et al. [33] studied the explosion characteristics of methane under unprotected conditions through experiments and CFD simulations, comparing the results with the FLACS (Flame Acceleration Simulation) software, providing significant insights for preventing gas explosions in coal mining ventilation systems. Song Sun et al. [34] conducted large-scale methane explosion ventilation experiments, discussing the impact of initial turbulence on pressure and flame development. Ze Wang et al. [35] demonstrated that the coupling suppression effect of the lateral venting port and the wire mesh on the flame is complementary through experiments. Di Chen et al. [36] conducted experiments that comprehensively captured the development of flow fields in public tunnels, contributing valuable insights for enhancing safety designs in tunnel spaces involving combustible gases. Ma Y et al. [37] explored explosion dynamics based on experimental validation and numerical simulations, offering important findings for the healthy development of hydrogen energy and improvements in green processes.

In summary, the research on flame characteristics and stability encompasses multiple aspects, ranging from theoretical models to practical experiments, covering flame behavior under various fuels, pressures, and geometric conditions. The aforementioned literature provides critical scientific foundations for understanding flame propagation mechanisms and their instabilities while also offering valuable references for improving safety designs and preventing explosion incidents. Future research should continue to deepen the understanding of the relationship between flame characteristics and stability, promoting the advancement of combustion science and engineering practices.

2.3. Numerical Simulation and Experimental Research on Venting Explosions

In recent years, significant progress has been made in the numerical simulation of and experimental research on venting explosions. Researchers have delved into various parameters and models to investigate phenomena such as flame instability, turbulence effects, and the influence of vent openings on flame shape deformation. These studies not only enrich the theoretical foundation of venting explosions but also provide crucial safety guidelines for industrial applications.

Canu et al. [38] proposed two empirical parameters to explain flame instability phenomena and the turbulence and flame shape deformation caused by vent openings. Mercx et al. [39] focused on the impact of vent opening area, pressure, ignition location, and configuration on the explosion process, emphasizing the role of obstacles. Molkov et al. [40,41] examined flame stretching and its effect on estimating deflagration–outflow interaction numbers, discussing the universality of the Le Chatelier–Brown principle in vented deflagrations.

Subsequent studies by Bauwens et al. [42–44] conducted experimental and numerical investigations on the behavior of hydrogen mixtures in enclosed spaces of varying sizes. They developed a three-dimensional fluid dynamics model based on large eddy simulation (LES), exploring how fuel concentration, ignition position, vent size, and obsta-

cles affect the pressure development of propagating flames. Notably, in their 2014 study, they found that initial turbulence primarily influences venting explosion overpressure by generating higher flame wrinkling, with less impact on the growth rate of wrinkles. Additionally, Ping Tang et al. [45] conducted a simulation of fuel–air vented explosions in a pipeline based on the k - ϵ turbulence model and the eddy dissipation concept (EDC) model. The results indicate that the explosion within the pipeline leads to a higher maximum pressure reduction; frictional resistance and gas column inertia play a secondary role in exacerbating the explosion violence; and the use of dual pipes can reduce the explosion severity. LI Qinhuo et al. [46] pointed out that the moment of weak panel rupture and the change in cavity volume are important factors affecting vacuum cavity explosions. Olivier Vermorel et al. [47] presented a new experimental and large eddy simulation database to research upscaling effects in vented gas explosions. WAN et al. [48] investigated the emission effects of side vent openings, noting that the relative position of obstacles to side vents significantly impacts venting effectiveness. He suggested placing side vents near flammable points in practical applications to enhance safety release effects. Yun Zhang et al. [49] emphasized the importance of numerical results in obtaining explosion parameters that are difficult to measure experimentally, highlighting that the coupling of explosion parameters plays a critical role during venting processes. Shigang Yang et al. [50] experimentally studied the influence between gas concentration and venting pressure and obtained a semi-empirical double-hump calculation model.

In summary, numerical simulation and experimental research have become increasingly vital in understanding and preventing venting explosions. These studies not only provide theoretical support for enhancing explosion safety but also promote technological advancements in related fields. Future research should continue to explore more complex environmental factors and new models to further improve the understanding and control of venting explosion phenomena.

2.4. Limitations and Challenges

Currently, the research on explosion loads during gas explosions under constrained venting conditions primarily focuses on parameters such as fuel reactivity, ignition location, vent conditions, initial flow fields, and obstacles. The widely used empirical formulas for predicting explosion venting loads are derived from these experiments, and their validity is limited to the range of experimental dimensions. Existing analytical methods often make approximations during the derivation process to simplify the analysis, which can result in significant discrepancies from real-world conditions. Additionally, a critical parameter in calculating the release of combustible gas during an explosion is the combustion velocity, which characterizes the chemical properties of the gas. Previous studies have introduced factors like combustion instability and turbulence coefficients, fitting these with specific venting parameters such as vent size, venting pressure, and container dimensions. However, accurate values for combustion instability and turbulence coefficients have not yet been determined experimentally, leaving the understanding of the dynamic disturbances and variations in the flow field during gas explosion venting processes incomplete. In structural design against gas explosion loads, there are no standardized criteria or manuals for determining gas explosion loads under venting conditions, leaving this area of explosion load determination still open to exploration.

In the overview of explosion pressure and its influencing factors, we recognize that the current models fail to account for the effects of various factors, particularly the simultaneous influences of external explosions and internal secondary explosions. The blast load is complex, often represented by a multi-peak pressure load curve, leading to different mechanisms for each peak. While previous experimental and theoretical studies have focused on the effects of numerous factors and the associated explosion hazards, there is a scarcity of research on classifying the multi-peak curves produced by variable physical mechanisms and understanding the characteristics of different types of curves. Addressing this gap, the study of explosion load characteristics of fuel–air mixtures in vented chambers

is highly significant, as it not only aims to fill this knowledge void but also provides detailed theoretical insights and practical references for optimizing explosion safety design. Vented explosion loads are classified into three typical types based on comprehensive literature research, and numerical modelling of these three models is conducted to investigate the explosion load characteristics.

2.5. Three Different Typical Vented Explosion Load Models

Understanding the different types of vented explosion load models is crucial for engineering safety and protective design. These models provide important insights into the combustion of fuel–air mixtures and the subsequent gas outflow processes. This section will discuss three typical vented explosion load models: the accumulation load model, the attenuation load model, and the interval jump load model. Each model exhibits unique pressure variation characteristics and is applicable to specific scenarios. First, the accumulation load model emphasizes the overpressure generated during combustion and its peak characteristics. Next, the attenuation load model focuses on the rapid pressure drop during the venting process. Finally, the interval jump load model illustrates multiple pressure fluctuations that occur in fuel-rich conditions. Analyzing these models establishes a theoretical foundation for understanding and mitigating the effects of vented explosions.

2.5.1. Survey of Methane–Air Mixture Vented Explosion Experimental Data

This survey of available experimental data is limited to methane–air mixture vented explosions with an initial atmospheric temperature and a ratio of the smallest to largest length of the chamber of more than 1/4. Dust explosions were also excluded from the present study. In these cases, the parameters, such as vessel shape, methane concentration, length-to-diameter ratio (L/D), ignition position, and vent positioning and type, are all given. A total of 89 sets of valid experimental data were collected (Cooper et al. [3], Harrison et al. [4], Mercx W. P. M [39], Jin Guo et al. [10], Fakandu et al. [8], Bauwens et al. [26], Bauwens et al. [43], Chao J et al. [6], Qin Fang et al. [51], Jiang Xiaohai et al. [52], Janovsky Bretislav et al. [53], Ferrara G. et al. [54], Proust Ch [55], Zhang Kai et al. [56]). The effects of the initial parameters, including the volume of the confined chamber, initial pressure, vented explosion pressure, fuel concentration, and ignition source position, were studied in the test. The overpressure peaks and corresponding time histories of the loads were recorded.

There are several possible overpressure peaks in methane–air mixture vented explosions, as Cooper discovered. The first overpressure peak is induced by the opening of the vented explosion plate. The second overpressure peak is caused by the flame reaching the relief opening. The third overpressure peak is due to the fuel–air mixture external explosion and the flame reaching the wall. The fourth overpressure peak is caused by oscillations due to combustion instability. Based on the relationship between the overpressure peaks mentioned above and the corresponding time of arrival of the overpressure peaks, the 46 curves are classified into the following three typical models: accumulation type, attenuation type, and interval jump type. These three blast load models are classified according to whether a higher explosion overpressure will be caused after the vented explosion. The indoor pressure dropped directly after the vented explosion of the attenuation type. A vented explosion of the accumulation type and the interval jump type would trigger a greater explosion overpressure. For the interval jump type, the indoor pressure would drop to atmospheric pressure for a while and then rise again due to the occurrence of a vented explosion. For the accumulation type, the indoor pressure drops slightly (but not to atmospheric pressure) and then continues to rise due to the occurrence of a vented explosion.

2.5.2. Accumulation Load Model

The loading curves shown in Figure 1 demonstrate the characteristics of the accumulation load model in a vented explosion. In this model, the overpressure rise induced by the fuel–air mixture combustion inside the chamber is more obvious than the overpressure drop induced by gas outflow from the vent after the venting plate fails. There may

be several peaks during the vented explosion process, which may decrease slightly and momentarily. However, the overall overpressure inside the vessel reaches the maximum pressure. According to the survey data, the loads in accumulation vented explosions often appear in cases with low vented explosion pressure and lean fuel combustion.

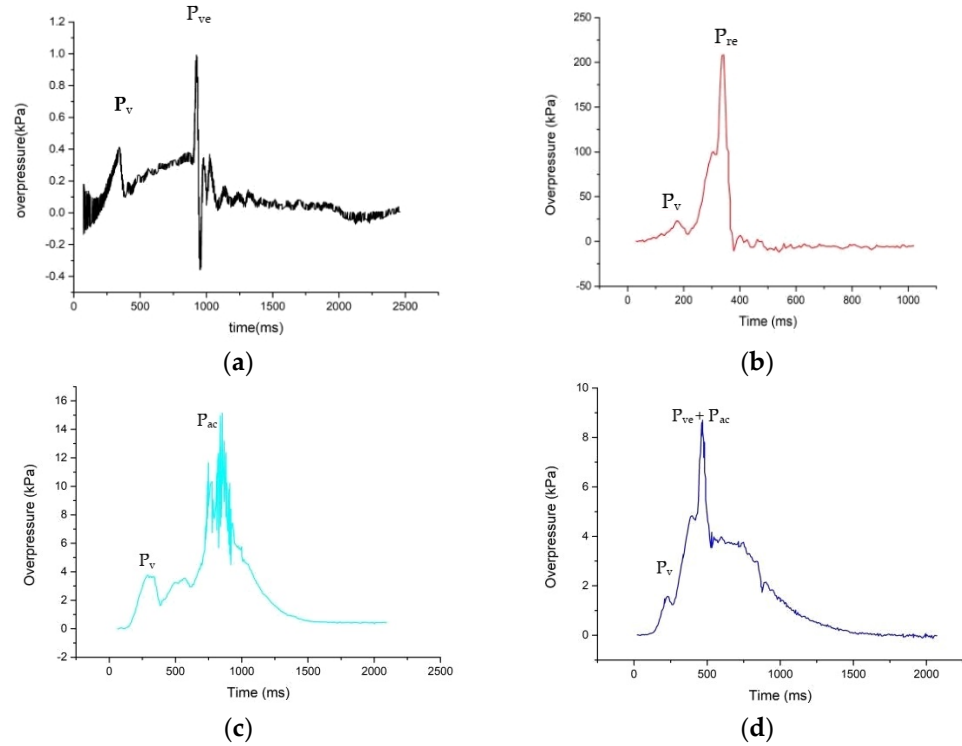


Figure 1. The characteristics of the overpressure-time profile in the accumulation load model. (a) Experimental data from Qin Fang et al. [51]; (b) Experimental data from Harrison et al. [4]; (c) Experimental data from Mercx et al. [39]; (d) Experimental data from Mercx et al. [39]. P_v , vented explosion. P_{ve} , overpressure peaks induced by external explosion. P_{re} , overpressure peaks induced by gas backflow. P_{ac} , peak oscillation due to unstable combustion.

2.5.3. Attenuation Load Model

The loading curves shown in Figure 2 display the characteristics of the attenuation load model. After the venting plate is opened in this model, the gas outflow from the vent is dominant, and the pressure drops sharply. According to the survey data, attenuation vented explosion loads often appear in cases with high vented explosion pressure, large vent area, or lean fuel combustion.

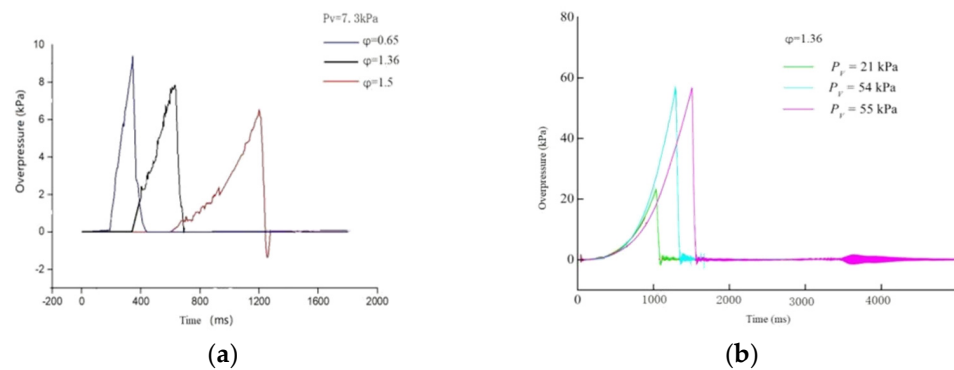


Figure 2. The characteristics of overpressure-time profile in the attenuation load model. (a) Experimental data from Qin Fang et al. [51]; (b) Experimental data from Qin Fang et al. [51]. P_v , vented explosion. ϕ equivalent.

2.5.4. Interval Jump Load Model

The loading curves shown in Figure 3 show the characteristics of the interval jump load model. In this model, the overpressure inside the chamber firstly rises and then drops to the normal pressure after venting. After that, the overpressure rise induced by the fuel–air mixture combustion inside the chamber and the pressure drop induced by gas outflow from the vented explosion channel are equal. The pressure is balanced. As the flammable gas surface rises, the fuel–air mixture combustion rapidly rises, and the pressure surges to form the second peak. In addition, the peak in oscillation is due to the instability of combustion. There may be more than two interval pressure rises in the interval jump load model. According to the survey data, the interval jump load model occurs in cases with fuel-rich combustion.

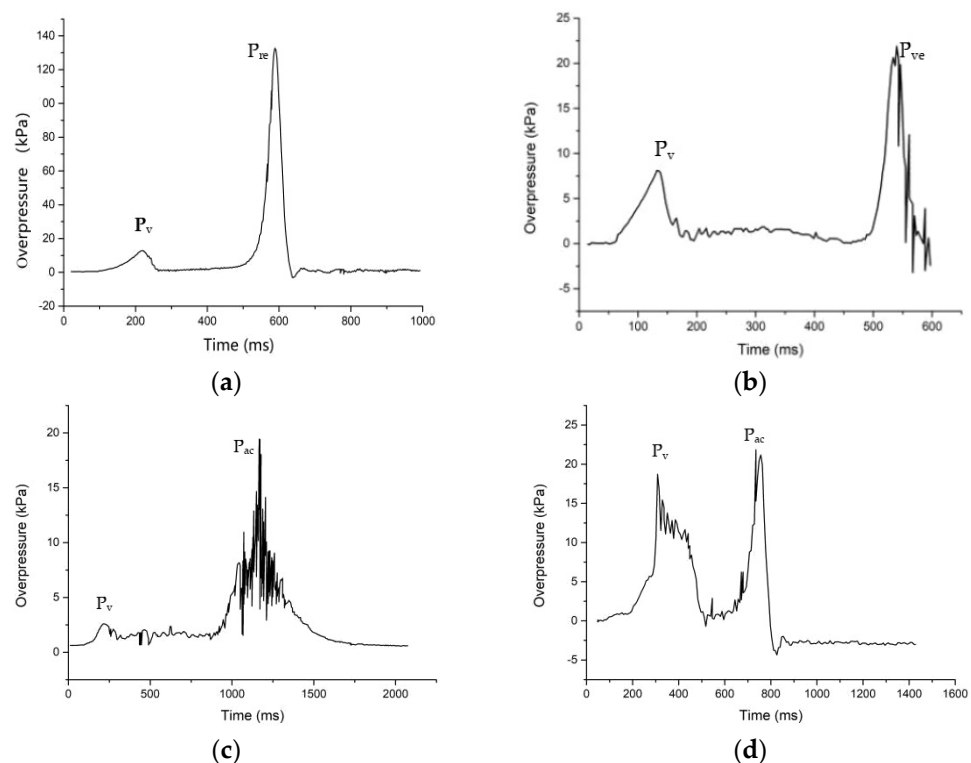


Figure 3. The characteristics of overpressure-time profile in the interval jump load model. (a) Experimental data from Qin Fang et al. [51]; (b) Experimental data from Cooper et al. [3]; (c) Experimental data from Mercx et al. [39]; (d) Experimental data from Harrison et al. [4]. P_v , vented explosion. P_{ve} , overpressure peaks induced by external explosion. P_{re} , overpressure peaks induced by gas backflow. P_{ac} , peak oscillation due to unstable combustion.

In our study, all three models indeed initiate ignition within the working area (chamber), as depicted in Figure 4a where the red dot marks the ignition point. This location represents a controlled environment for initial combustion, aligning with your comment on typical ignition locations. Under ideal conditions, once the vent is opened, the fuel–air mixture inside the chamber would be fully combusted, releasing only burnt gases at high pressure. In practice, however, the vent opens at a designated pressure threshold before full combustion occurs. At this point, some unburnt gases escape through the vent, as shown in Figure 4b. As the vent opens, the flame front stretches toward the vent, igniting the unburnt gases that have already exited the chamber and causing an external explosion, illustrated in Figure 4c. This phenomenon has also been observed in the experiments by Cooper et al. [3], Harrison et al. [4], and Qi Fang et al. [51]. In all three models investigated, there exists the possibility for combustion within the chamber (working area) to propagate to the outdoor ventilated area, reflecting the potential for both indoor and outdoor explosion dynamics within the same setup.

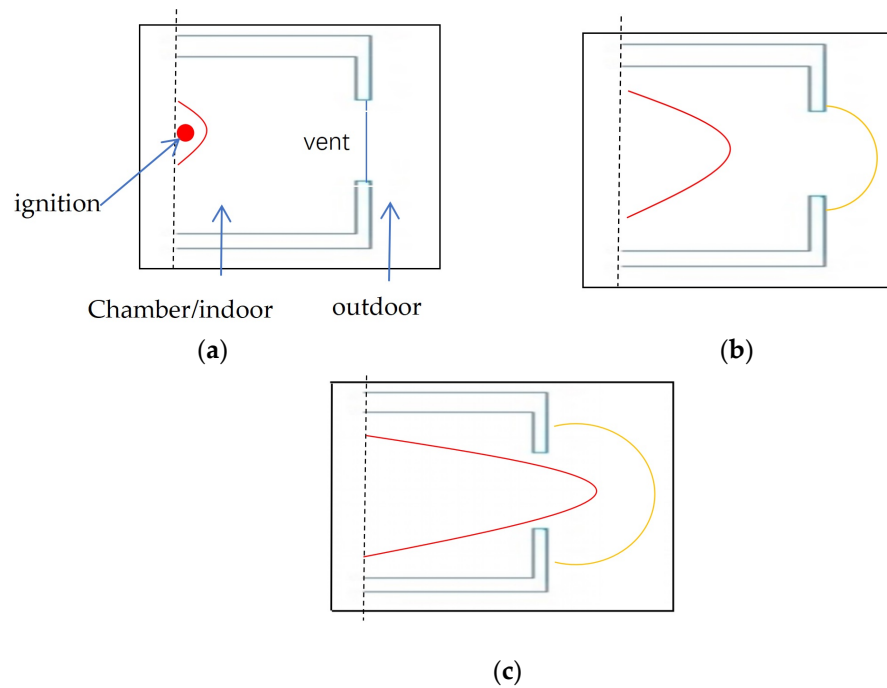


Figure 4. Schematic diagram of fuel–air mixture explosion in a vented chamber (the red line represents the flame front, while the orange line represents the release of combustible gases outdoors). (a) The stage of fuel–air mixture ignition; (b) The stage of flame front expansion towards the vent; (c) The flame front flowout and ignition of the outdoor fuel–air mixture.

3. Theory of Numerical Modeling of Vented Explosion Load Models

The basic gas explosion equations are the mass conservation equation, energy conservation equation, and Navier–Stokes equations in the simulation. The numerical analysis was performed by the software VENTEX-GUI (Version number: 2020), which solves the Navier–Stokes equations along with the equations describing conservation of mass and energy for a mixture of compressible ideal gases. The governing equations are written below.

Mass conservation equation [57]:

$$\frac{\partial \rho}{\partial t} + \nabla \cdot (\rho \mathbf{U}) = S_{\rho} \quad (1)$$

Energy conservation equation [57]:

$$C_p \left[\frac{\partial (\rho T)}{\partial t} + \nabla \cdot (\rho \mathbf{U} T) \right] = -\nabla \cdot \mathbf{q} + \left[\frac{\partial p}{\partial t} + \mathbf{U} \cdot \nabla p \right] + \tau : \nabla \mathbf{U} + S_T \quad (2)$$

Navier–Stokes equations [57]:

$$\frac{\partial (\rho \mathbf{U})}{\partial t} + \nabla \cdot (\rho \mathbf{U} \mathbf{U}) = \nabla \cdot \boldsymbol{\tau} - \nabla p + S_U \quad (3)$$

where p is the pressure, ρ is the density, T is the temperature, $\boldsymbol{\tau}$ is the tensor of viscous stress ($= \mu \dot{\boldsymbol{\gamma}} - (\frac{2}{3}\mu - K)(\nabla \cdot \mathbf{U})\boldsymbol{\delta}$), \mathbf{U} is the velocity vector, M is the effective viscosity, K is the dilatational viscosity, $\boldsymbol{\delta}$ is the unit tensor, C_p is the specific heat at ordinary pressure, k is the effective thermal conductivity, S_U is the source term of momentum equation, $\dot{\boldsymbol{\gamma}}$ is the rate-of-strain tensor ($= (\nabla \mathbf{U}) + (\nabla \mathbf{U})^T$), \mathbf{Q} is the heat flux vector ($= -k\nabla T$), S_T is the source term of the energy equation, and S_{ρ} is the source term of the mass conservation equation.

Turbulence is described by a two-equations model; one is the dissipation rate ϵ equation, and the other is the turbulence k equation, which constitutes the conservation equation [57]:

$$\frac{\partial(\rho\varepsilon)}{\partial t} + \nabla \cdot (\rho \mathbf{U} \varepsilon) = \nabla \cdot \left(\mu_t + \frac{\mu_t}{\sigma_\varepsilon} \right) \nabla \varepsilon + \frac{\varepsilon}{k} [C_{\varepsilon 1} (P_k + P_b) - C_{\varepsilon 2} \rho \varepsilon] - \left(\frac{2}{3} C_{\varepsilon 1} - C_{\varepsilon 3} \right) \rho \varepsilon \nabla \cdot \mathbf{U} + S_\varepsilon^V \quad (4)$$

$$\frac{\partial(\rho k)}{\partial t} + \nabla \cdot (\rho \mathbf{U} k) = \nabla \cdot \left(\mu_t + \frac{\mu_t}{\sigma_k} \right) \nabla k + P_k + P_b - \rho \varepsilon - \frac{2}{3} \rho k \nabla \cdot \mathbf{U} + S_k^V \quad (5)$$

where P_k is the mechanical production rate of k ($=\mu_t \dot{\gamma} : \nabla \cdot \mathbf{U}$); P_b is the buoyancy production rate of k ($=\mu_t \beta \frac{\rho \nabla T}{\sigma_h}$); σ_h is the turbulent schmidt number; ε is the dissipation rate of k ; σ_k is the Prandtl number for turbulent diffusion of k ($=1$); S_k^V and S_ε^V are the source term due to vegetation canopy; and $C_{\varepsilon 1}$, $C_{\varepsilon 2}$, $C_{\varepsilon 3}$, σ_k , and σ_ε are the k - ε model constants.

In our study, we did not employ mechanical ventilation. Before the vent is opened, the indoor environment is assumed to be in a sealed state, with the air remaining at rest. After the vent opens, airflow is generated due to the pressure differential between the inside and outside. The turbulence calculated in our study results from changes in the flow field caused by the opening of the vent, and we did not consider the turbulent dynamic mode of air movement through mechanical ventilation.

The fuel–air mixture combustion reaction provided the heat. The process of heat addition is regarded as an explicit one-step conversion of the fuel–air mixture to the products. Conservation of species concentration is as follows [57]:

$$\frac{\partial(\rho y_i)}{\partial t} + \nabla \cdot (\rho \mathbf{U} y_i) = \nabla \cdot D_i \nabla (y_i) + S_i \quad (6)$$

where y_i is the mass fraction of species i , D_i is the effective diffusion coefficient for species m , and S_i is the source term for the species m equation.

The burning velocity is illustrated by the modification of the BML model (modify Bray–Moss–Libby model) [58]:

$$\omega = C_1 \bar{\rho} \Gamma_k A_g U_t (1 + \tau) \frac{\bar{c}(1 - \bar{c})}{(1 + \tau \bar{c})} \quad (7)$$

$$\bar{\rho} = \frac{\rho_R}{(1 + \tau \bar{c})} \quad (8)$$

$$\tau = \left(\frac{T_b}{T_u} - 1 \right) \quad (9)$$

where Γ_k is the normalized tensile ratio, τ is the ratio of gas expansion, C_1 is the coefficient from experience, \bar{c} is the overall progress variable, T_b is the temperature of the combustion products, T_u is the temperature of the unburned gas, and $\bar{\rho}$ is the normalized density of the combustible gas mixture. The fuel–air mixture turbulent combustion speed is computed according to the gas viscosity, laminar flame speed of the local fuel–air mixture, turbulent mean fluctuation velocity, and integrated turbulent length scale.

4. The Three Typical Vented Explosion Loads Simulation Study and Discussion

4.1. Modeling and Validation

In order to prove the accuracy of simulation by experiment, the dimensions of the chamber used in the simulations, i.e., $2 \text{ m} \times 2 \text{ m} \times 3 \text{ m}$, were like those in Qin Fangs' sets [51]. In those experiments, the room was packed into a methane–air mixture with a volume concentration of 6.5–13.5%. According to the target methane concentration, the amount of methane required was calculated, and then, the amount of methane flowing into the room was controlled by the flow meter and the gas cylinder output time. An ignition source with an energy of approximately 100 mJ was placed in the center of the room. A square explosion vent (size $80 \text{ cm} \times 80 \text{ cm}$) was placed at the center of the forefront wall, and the vented surface was covered with glass or film of different strengths to adjust the vented pressure, as shown in Figure 5. An infrared gas measuring instrument with a measurement accuracy of 0.1% and a range of 0–15 vol.% was used to measure the

concentration of methane. A blast-proof fan was fixed in the combustion chamber. The fan flow of the blower was $0.8 \text{ m}^3/\text{s}$, and continuous stirring was conducted for 20–30 min to confirm a well-distributed fuel–air composition. The pressure sensor was installed on the center of the back wall. In the experiment, four sets of methane–air mixture vented explosion experiments were conducted. The methane concentration and vent covers are variable. The concentration and vented pressure values of cases No. 1–No. 4 are listed in Table 1. In the experiments, variable strength venting covers were applied to adjust the vented overpressure. Therefore, a constrained vent was designed, and rigid insulation walls were constructed. The ignition was arranged in the enclosure center. The overpressure–time history was measured at the center of the back wall, which is opposite the vented wall.

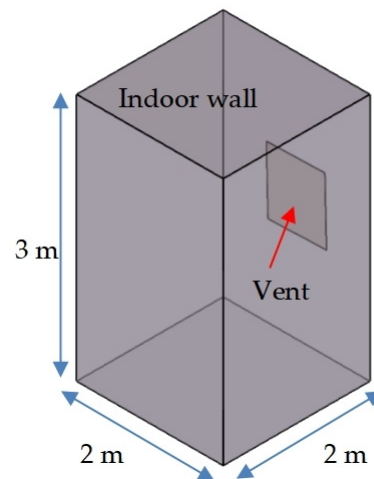


Figure 5. Physical model of numerical computation.

Table 1. The CH_4 concentration and vented pressure of cases 1–4.

No.	Concentration (V/V%)	Vented Pressure (kPa)
1	10.5	0.3
2	6.5	0.3
3	10.5	7.3
4	12.5	54

4.1.1. Mesh and Sensitivity Analysis

Figure 6 shows the 3D grid division of the calculation area, with the gas venting area dimensions of $5000 \text{ mm} \times 3000 \text{ mm} \times 4000 \text{ mm}$, room dimensions of $2000 \text{ mm} \times 2000 \text{ mm} \times 3000 \text{ mm}$, and cell dimensions of $50 \text{ mm} \times 50 \text{ mm} \times 60 \text{ mm}$; the whole cells is 480,000. We conducted sensitivity tests using three mesh sizes: $100 \text{ mm} \times 100 \text{ mm} \times 100 \text{ mm}$, $50 \text{ mm} \times 50 \text{ mm} \times 60 \text{ mm}$, and $30 \text{ mm} \times 30 \text{ mm} \times 30 \text{ mm}$. The 10% error in our simulations is specifically related to the pressure values. The simulation results for the first mesh size showed an error greater than 10% compared to the experimental data in terms of pressure. Therefore, this size was not adopted. In contrast, the results for the latter two mesh sizes had errors of less than 10% compared to the experimental data regarding pressure, which are considered within an acceptable range. Considering both computational accuracy and time cost, we ultimately selected the $50 \text{ mm} \times 50 \text{ mm} \times 60 \text{ mm}$ mesh size.

The purpose of our mesh sensitivity testing was to ensure that the pressure from the numerical simulations did not exceed a 10% error compared to the experimental data while minimizing computation time. From an engineering application perspective, the $50 \text{ mm} \times 50 \text{ mm} \times 60 \text{ mm}$ mesh size meets these requirements. Regarding the potential refinement, thickness, element count, and other factors mentioned by the reviewer, we will strive to address these aspects in future work, as computational capabilities allow.

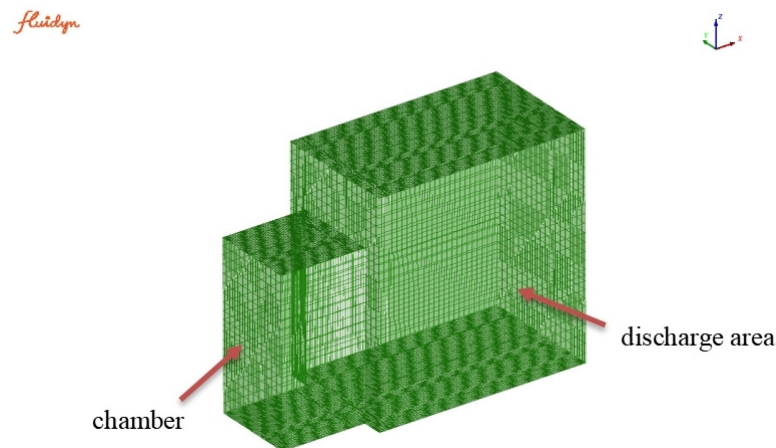


Figure 6. 3D meshes for the chamber and discharge areas.

It is worth mentioning that, among the three grid sizes mentioned above, we first conducted simulations using a grid size of $100\text{ mm} \times 100\text{ mm} \times 100\text{ mm}$. With this grid size, the element count was 72,000. The simulation results showed that the peak explosion pressure was 15% higher than the experimental value, which was greater than the 10% error that we had set.

Next, we refined the grid, reducing the grid thickness from 100 mm to 30 mm, resulting in a grid size of $30\text{ mm} \times 30\text{ mm} \times 30\text{ mm}$. With this refinement, the element count increased to 8,000,000. The simulation results showed that the peak explosion pressure was within the 10% error compared to the experimental value, which met our expectations. However, the total number of elements was very large, leading to excessively long computational times and inefficiency.

Finally, we adjusted the grid thickness and chose a grid size of $50\text{ mm} \times 50\text{ mm} \times 60\text{ mm}$, resulting in an element count of 480,000. The simulation results showed that the peak explosion pressure was within the 10% error compared to the experimental value, and the computational time was reasonable. Based on these factors, we ultimately selected this grid size for further simulations.

4.1.2. Calculation Model Validation

In order to test and verify the validity of the model, the VENTEX-GUI numerical calculation results acquired were compared with Qin Fangs' experimental results [51]. We have validated the accuracy of the model by comparing the peak pressure values and their arrival times from both experimental and simulation results, setting an acceptable error margin of less than 10%. The 10% error in our simulations is specifically related to the pressure values.

Figure 7 demonstrates that the VENTEX-GUI simulation calculation is approximately consistent with the No. 1 experimental results. The figure shows that the premixed gas inside the chamber first undergoes a relatively slow initial combustion process, during which the pressure inside the chamber gradually rises. Venting occurs both in the experiment and simulation when the overpressure in the vessel increases to the cracking overpressure after igniting for 0.22 s. Subsequently, the overpressure in the chamber drops. The pressure rises to the fourth peak at approximately 0.6 s in the experiment and at approximately 0.55 s in the simulation. The pressure is 67 kPa in the simulation, which is 6.9% lower than that in the experiment. The numerical analysis model is effective for reproducing the test results.

Figure 8 shows the evolution of the contours of temperature and flame in case 1. The premixed fuel is combusted in the closed chamber, and the overpressure increases before the vent disc opens. The flame front at variable times is shown in Figure 8 with a red curve. As shown in Figure 8b, the near-spherical flame surface is disturbed toward the vent after the vent disc is broken. The gas outflow from the vent is predominant, and there is a slight drop in pressure. Then, as shown in Figure 8c, the flame front extends outside the chamber

and ignites the previously released combustible gas. Since the methane concentration is reduced after the released combustible gas is mixed with outdoor air, outdoor combustion is mild, and the second pressure peak is not apparent. Due to the release of indoor gas, there is a strong indoor gas disturbance, and a gas backflow phenomenon occurs in the process of gas entrainment during an outdoor explosion. Finally, the residual methane–air mixture in the chamber combusts completely at 625 ms to produce the maximum pressure value.

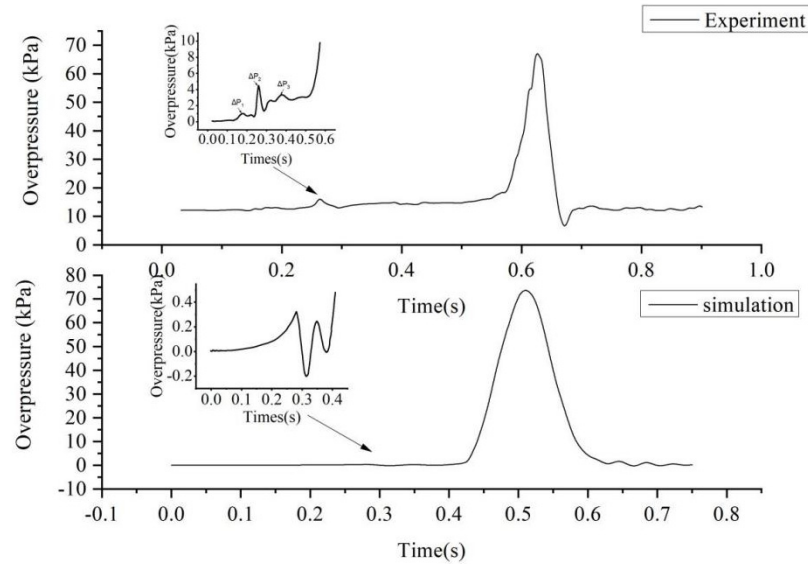


Figure 7. Overpressure-time history inside the chamber of case 1.

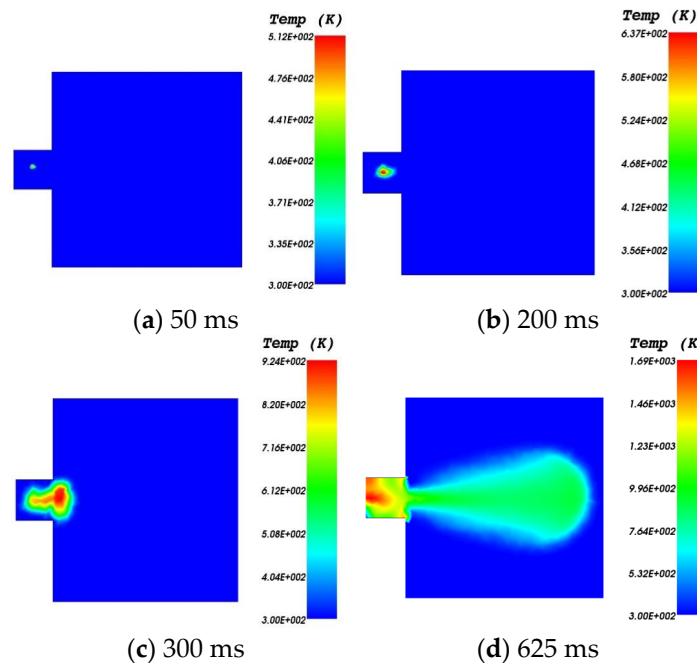


Figure 8. Evolution of the contours of temperature and flame front (red curve) in case 1.

4.2. Vented Explosion Load Model Analysis of Cases 1–4

The vented explosion load model analysis is investigated from the simulation results of cases 1–4. The explosion overpressure peaks induced by variable physical mechanisms were detected in the different cases. The overpressure-time histories inside the chamber for case 1, case 2, case 3, and case 4 are exhibited in Figures 7 and 9a–c, individually.

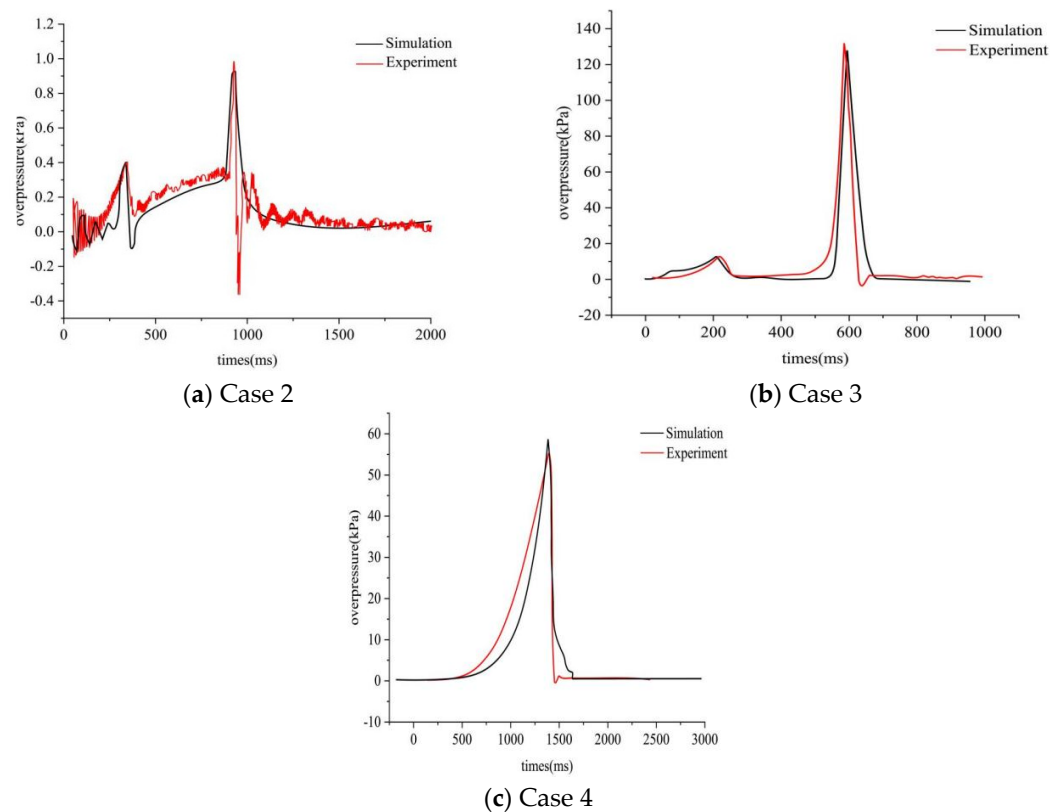


Figure 9. Pressure-time history inside the chamber of cases 2–4.

Figures 7 and 8 show the overpressure-time curve and the flame evolvement of case 1, respectively, in an empty enclosure filled with a 10.5% volume concentration of methane ignited in the center of the room. The explosion relief pressure is 0.3 kPa. The vented explosion load model of case 1 is the interval jump load model.

Figure 9a shows the pressure-time curve of case 2 in an empty enclosure filled with a 6.5 v/v methane–air mixture ignited in the center of the room. The explosion relief pressure is 0.3 kPa. The overpressure peaks in the experiment and simulation were both approximately 1 kPa, indicating that the fuel–air mixture was slowly burning inside the vessel. The vented explosion occurred at approximately 0.3 s. Then, the experimental overpressure continued to rise slowly, while the simulation showed an oscillation phenomenon. However, overall, the pressure still presented an accumulation and rise process in the simulation. The second overpressure peak appeared in the experiment at approximately 0.9 s, and the simulation showed a second overpressure at approximately 1 s. The vented explosion load model of case 2 is the accumulation blast load model.

Figure 9b exhibits the pressure-time curve of case 3 in an empty enclosure filled with a 10.5% volume concentration of methane ignited in the center of the room. The explosion relief pressure is 7.3 kPa. The comparison between the experiment and the simulated explosion overpressure results of this type is exhibited in Figure 7. The numerical calculation results were consistent with the experimental results. As the figure shows, the most important feature of this type of overpressure curve is that there are two distinct overpressure peaks. The vented explosion load model of case 3 is the interval jump load model.

Figure 9c shows the pressure-time curve of case 4 in an empty enclosure filled with a 12.5% volume concentration of methane ignited in the center of the room. The explosion relief pressure is 54 kPa. As the figure shows, in the case of the 12.5% methane concentration and the 54 kPa vented explosion pressure, there is only one overpressure peak. The experiment was consistent with the simulation results. The vented explosion load model of case 4 is the attenuation blast load model.

4.3. The Characteristics Analysis of the Interval Jump Load Model

The simulation results reported and discussed in this section are focused on the characteristics of case 1 and case 3. The vented explosion load models of these two cases are interval jump load models.

For case 1, the maximum turbulent strength of the gas inside the chamber varies with time, as exhibited in Figure 10. The turbulent strength of the gas mixture inside the chamber varied significantly near the vent after venting. The turbulent strength increased from the original 0.0001 J/kg to 1.73 J/kg, which is an increase of 17,300 times, indicating that the turbulent strength changed greatly before the fourth peak occurred. The spatial distribution of turbulence intensity inside the chamber is shown in Figure 11. The increase in the turbulent strength will act on the combustion reaction zone, causing disturbances in the fluid of the fuel–air mixture combustion reaction zone. As a result, the fuel–air mixture combustion rate and energy release efficiency increased, as did the pressure. In turn, the disturbance of the fluid became greater, and the turbulent strength was higher. The interplay between the fluid disturbance and the combustion resulted in an intensified combustion and caused the overpressure to rise rapidly. When the methane concentration is gradually reduced, the energy release cannot compensate for the energy loss process, even if the turbulent strength is high, making the pressure gradually decrease, resulting in an overpressure peak (P₄ of Figure 7). The density of chemical species-CH₄ varies with time, as shown in Figure 12. The density of chemical species-CH₄ at the first peak time and second peak time is presented in Figure 12b,c, separately. However, the pressure was still an accumulation and rise process overall in both the experiment and simulation.

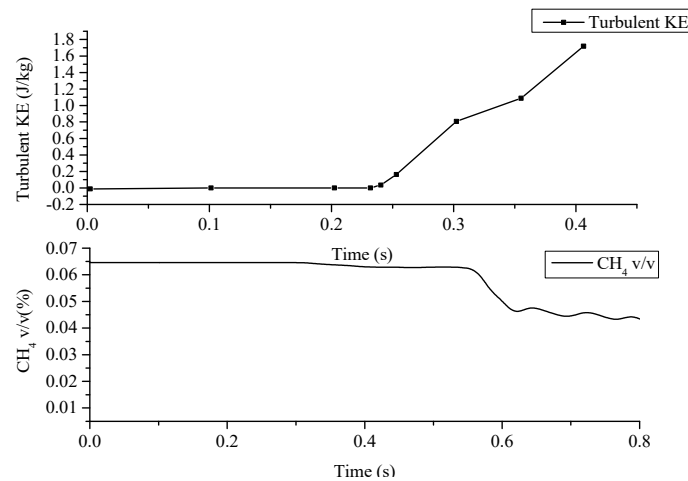


Figure 10. The maximum turbulence (top) and volume fraction of CH₄ (bottom) over time of case 1.

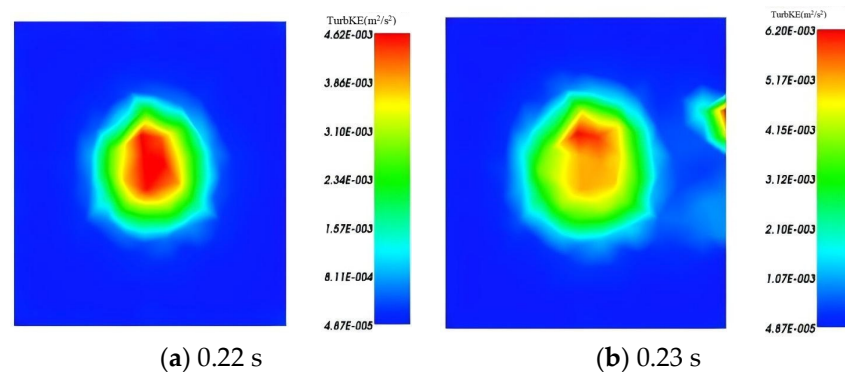


Figure 11. Cont.

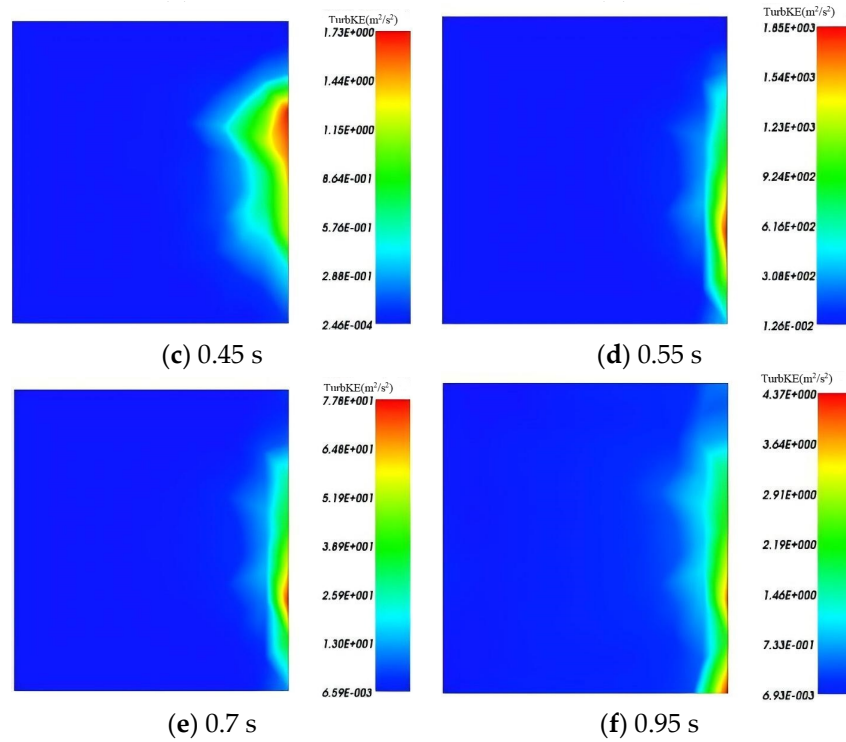


Figure 11. The spatial distribution of turbulence intensity inside the chamber (case 1).

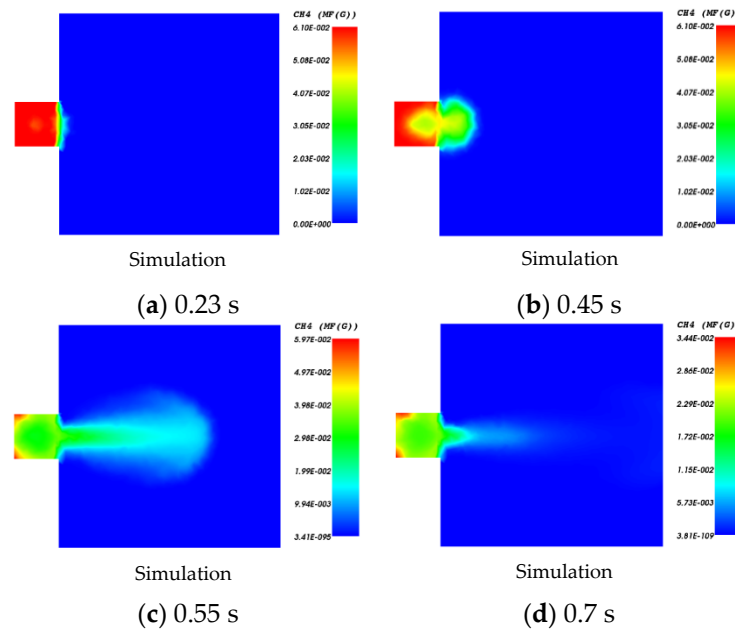


Figure 12. The spatial distribution of the density of chemical species-CH₄ (case 1).

The spatial distribution of airflow velocity (case 1) is exhibited in Figure 13. The airflow velocity was relatively low at the initial moment indoors. As the combustion progressed, it increased to 0.25 m/s at 0.2 s. The airflow velocity near the vent increased to 3.5 m/s after venting at 0.23 s. As the indoor pressure was higher than the outdoor pressure, a large amount of combustible gas indoors was released from the vent during the vented explosion. The direction of the airflow reversed due to the ignition of the external combustible gas, which was released from the vent. The reversed airflow velocity was 1.2 m/s at that moment (0.45 s). Then, the remaining combustible gas indoors burned

violently, the pressure increased, and the airflow velocity increased to approximately 68 m/s at 0.55 s. Finally, the airflow velocity decreased gradually at the end of burning.

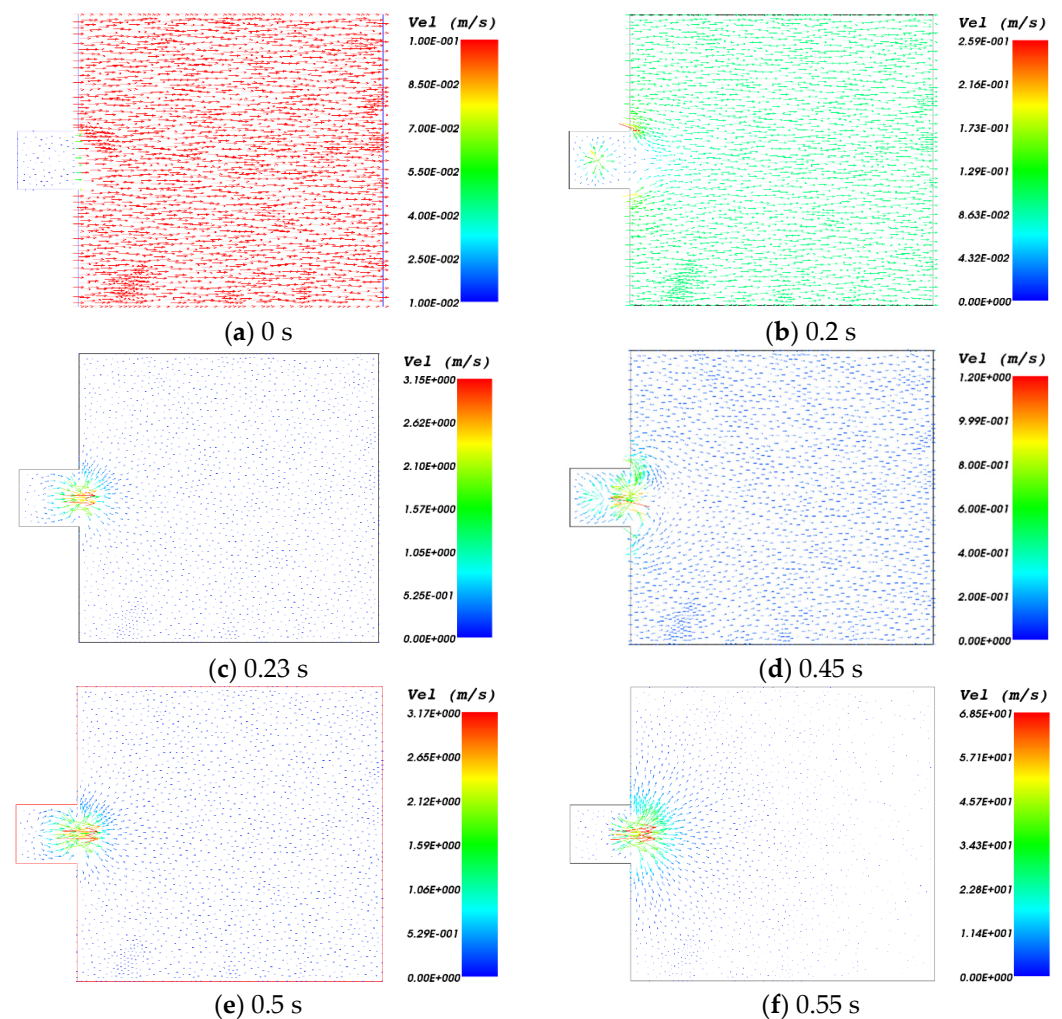


Figure 13. The spatial distribution of airflow velocity (case 1).

For case 3, the maximum turbulent strength of the gas inside the chamber varies with time. The turbulent strength increased from 0.0001 J/kg to 62.2 J/kg from 0 s to 0.5 s before the second overpressure rise, which was an increase of 622,000 times. This is because the instability of the flame itself resulted in an increase in turbulent strength. For example, thermal diffusion and other chemical kinetic reasons can cause the gas flow to increase. The velocity gradient between the gas burning at a high temperature and the unburned low-temperature gas will generate a shear force, deforming the flame front and forming a small-sized vortex, increasing the touch surface between the flame face and the fuel–air mixture. In addition, due to the vented explosion, the difference between the internal overpressure and external overpressure, along with the temperature difference, the gas flowed out from the chamber at a high speed, which would inevitably cause the turbulent strength to increase rapidly in a short period of time. The turbulent strength increased by a hundred times from 0.4 s to 0.55 s during the vented explosion.

4.4. The Characteristics of the Accumulation Load Model

The simulation results reported and discussed in this section are focused on the characteristics of case 2. The vented explosion load model of case 2 is the accumulation load model.

The maximum turbulent strength of the gas inside the chamber varies with time, as shown in Figure 14. It can be observed in the figure that the turbulent strength increased from 0.0001 J/kg to 0.3 J/kg in the early stage of combustion, which is an increase of 3000 times. After the vent plate failed, the turbulent strength increased from 0.3 J/kg to 9.89 J/kg, which is an increase of 33 times. Although the turbulent strength can improve the fuel–air mixture reaction rate and the energy release efficiency of the combustible gas, the combustion is not severe due to the low methane concentration. In these circumstances, the interplay between the fluid and the fuel–air mixture reaction is not obvious and cannot generate explosions.

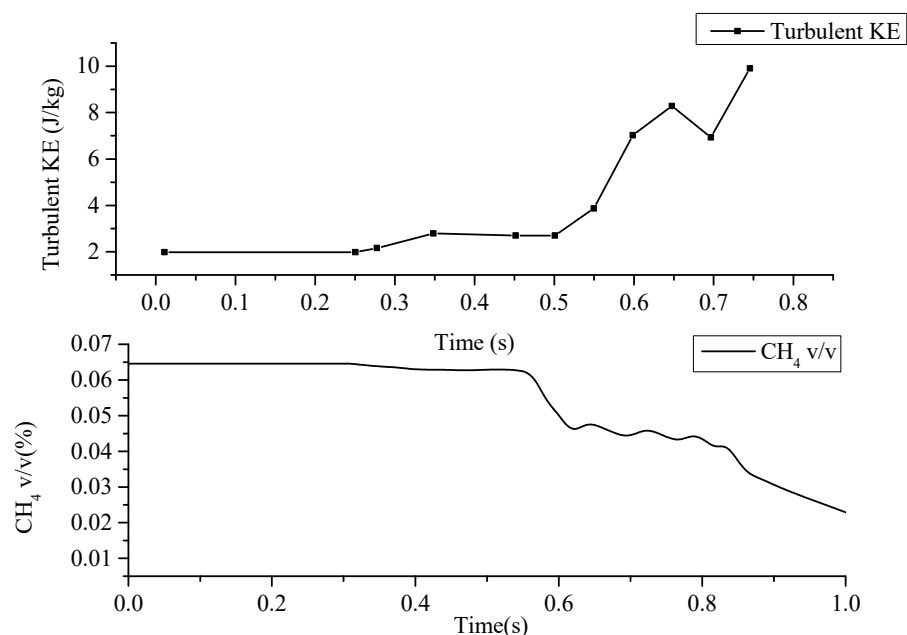


Figure 14. The maximum turbulence (**top**) and volume fraction of CH₄ (**bottom**) over time (case 2).

4.5. The Characteristics of the Attenuation Load Model

The simulation results reported and discussed in this section are focused on the characteristics of case 4. The vented explosion load model of case 4 is the accumulation load model.

The turbulent strength increased from the original 0.0001 J/kg to 3 J/kg, which increased rapidly in a short period of time when the vented explosion occurred, and the pressure rapidly decreased after the vented explosion. The biggest feature of the attenuation model is that there is only one overpressure peak. The reason for the formation of this overpressure peak is that the high vented explosion pressure caused a large consumption of methane gas in the room before the vented explosion occurred. When the vented explosion occurred at approximately 1.3 s, the residual methane gas in the room was already low. Even if the turbulent strength caused by the vented explosion changed drastically, there was not enough methane gas to form a subsequent intense combustion or even an explosion.

5. Discussion and Conclusions

The advances in the research on the explosion load characteristics of the fuel–air mixture in vented chambers are reviewed herein. Based on the historical research on vented explosions by analytical, experimental, and numerical approaches, three important aspects can be identified. Explosion pressure and influencing factors, flame characteristics and stability research, and numerical simulation and experimental research on venting explosions are detailed, respectively. The studies focused on the influences of various factors and the resulting explosion hazard. There are few studies on the classification of the multi-peak curves produced by varying physical mechanisms and the characteristics of the different types of curves. Vented explosion loads are classified into three typical

types based on comprehensive literature research. These models are the accumulation load model, attenuation load model, and interval jump load model.

Numerical analyses have been performed to explain the formation mechanism of these load models. The concept of the interaction between the fluid and chemical reaction could be adopted to explain the mechanism of the loads generated by a venting gas explosion, in which the loads are related to the venting pressure and fuel concentration. For methane at 10.5% v/v and 7.3 kPa vented pressure, which is related to the interval jump load model, the turbulence intensity increases significantly, and the chemical reaction rate and energy release efficiency are enhanced with increasing turbulence; then, the pressure also obviously increases. In turn, the disturbance of the fluid becomes greater, and the turbulent strength is higher. For methane at 6.5% v/v and 7.3 kPa vented pressure, which is related to the attenuation load model, as the turbulence intensity becomes high, the chemical reaction and pressure are low due to the lack of fuel. In this case, the explosion overpressure peak tends to ascend when the intensity of the fluid disturbance increases due to the venting pressure increasing at a constant initial gas concentration. When the venting pressure reaches tens of kPa, the overpressure variable on both sides of the vent increases sharply, and the amount of combustible gas released is very large. After venting, the amount of indoor combustible gas is insufficient, severe combustion is difficult to maintain, and the explosion load mode becomes the attenuation load model.

The main parameters affecting the explosion venting of indoor gas explosions include the type of combustible gas, gas concentration, vent area, venting pressure, and ignition source. Under constant conditions of the ignition source and vent area, the combustible gas concentration and venting pressure directly influence the explosion pressure within the chamber. Ideally, when the vent opens, all the combustible gas in the chamber has been fully burned, resulting in high pressure with only burned gas flowing out. However, in practice, to protect the equipment and facilities inside the chamber, the vent opens when the chamber pressure reaches its design value. At this point, some unburned gas may still remain, which can lead to a situation where the flame front is stretched towards the vent. When this deformed flame front exits the vent, it ignites the previously released combustible gas, resulting in an external explosion. Therefore, while designing the venting pressure, it is crucial to ensure that it meets the requirements for protecting internal equipment while minimizing the risk of external explosions. This highlights the trade-offs that must be carefully managed in safety design.

This study has made some progress in researching indoor gas explosion venting models. However, to achieve the goal of quickly and simply predicting indoor gas explosion venting pressures for blast-resistant design and disaster response, further efforts are needed in both theoretical research and engineering applications. In terms of theoretical research, it is essential to establish a calculation model for venting loads in vented gas explosions and to investigate how variations in flow fields under different real-world scenarios affect explosion venting loads. The rectangular theoretical model developed in this paper should be extended to irregular-shaped scenarios to analyze how building structures influence explosion loads. On the engineering applications side, to enhance the speed and accuracy of damage effect assessments under the influence of indoor gas explosion venting pressures, it is crucial to continuously improve experimental and numerical calculations of structural deformation and failure due to vented explosion. This will provide a solid basis for blast-resistant design.

In summary, the process of gas explosion venting is complex, involving principles of chemical reaction kinetics and fluid mechanics, which require further investigation. In particular, there is a need for research on how venting influences the turbulence level of gases, as this directly affects the combustion rate of flammable gases and, consequently, the explosion pressure. Since turbulence remains a significant challenge in this field, there is still much work to be conducted in this area.

Author Contributions: Conceptualization, X.L.; Investigation, X.L.; Methodology, Z.W.; Software, J.C. and Y.L.; Validation, C.L.; Writing—original draft, X.L.; resources, H.Z.; Writing—review and editing, H.A. All authors have read and agreed to the published version of the manuscript.

Funding: The authors would like to acknowledge the financial support of the Yunnan Fundamental Research Projects (grant NO. 202401CF070138). This study was also, in part, supported by the National Key Research and Development Plan of China (grant No. 2021YFC3001204), Science Research Project of Yunnan Provincial Department of Education (Grant No. 2023J0157 and No. 2022J0066), Kunming University of Science and Technology Talent Introduction and Research Start up Fund Project (grant NO. 241120230016), and Yunnan Province “Caiyun” Postdoctoral Innovative Project Plan (No. CG24056E004A).

Data Availability Statement: The original contributions presented in the study are included in the article, further inquiries can be directed to the corresponding author.

Conflicts of Interest: The authors have no relevant financial or nonfinancial interests to disclose.

References

1. UFC 3-340-02; Structures to Resist the Effects of Accidental Explosions. USA Criteria, Unified Facilities: Las Vegas, NV, USA, 2008.
2. TNO Yellow Book CPR 14E: Committee for the Prevention of Disasters. 2005. Available online: <https://studylib.net/doc/25642133/tno-yellow-book> (accessed on 7 January 2024).
3. Cooper, M.G.; Fairweather, M.; Tite, J.P. On the mechanisms of pressure generation in vented explosions. *Combust. Flame* **1986**, *65*, 1–14. [[CrossRef](#)]
4. Harrison, A.J.; Eyre, J.A. External explosions as a result of explosion venting. *Combust. Sci. Technol.* **1987**, *52*, 91–106. [[CrossRef](#)]
5. Bauwens, C.R.; Chaffee, J.; Dorofeev, S. Effect of Ignition Location, Vent Size, and Obstacles on Vented Explosion Overpressures in Propane-Air Mixtures. *Combust. Sci. Technol.* **2010**, *182*, 1915–1932. [[CrossRef](#)]
6. Chao, J.; Bauwens, C.R.; Dorofeev, S.B. An analysis of peak overpressures in vented gaseous explosions. *Proc. Combust. Inst.* **2011**, *33*, 2367–2374. [[CrossRef](#)]
7. Taveau, J. Correlations for blast effects from vented dust explosions. *J. Loss Prev. Process Ind.* **2010**, *23*, 15–29. [[CrossRef](#)]
8. Fakandu, B.M.; Andrews, G.E.; Phylaktou, H.N. Vent burst pressure effects on vented gas explosion reduced pressure. *J. Loss Prev. Process Ind.* **2015**, *36*, 429–438. [[CrossRef](#)]
9. Molkov, V.; Bragin, M. Hydrogen–air deflagrations: Vent sizing correlation for low-strength equipment and buildings. *Int. J. Hydrogen Energy* **2015**, *40*, 1256–1266. [[CrossRef](#)]
10. Jin, G.; Wang, C.; Li, Q.; Chen, D. Effect of the vent burst pressure on explosion venting of rich methane-air mixtures in a cylindrical vessel. *J. Loss Prev. Process Ind.* **2016**, *40*, 82–88.
11. Shao, H.; Jiang, S.; Wu, Z.; Wang, K. Application and effect of negative pressure chambers on pipeline explosion venting. *J. Loss Prev. Process Ind.* **2016**, *41*, 8–17. [[CrossRef](#)]
12. Makarov, D.; Hooker, P.; Kuznetsov, M.; Molkov, V. Deflagrations of localised homogeneous and inhomogeneous hydrogen-air mixtures in enclosures. *Int. J. Hydrogen Energy* **2018**, *43*, 9848–9869. [[CrossRef](#)]
13. Yu, M.; Wan, S.; Zheng, K.; Guo, P.; Chu, T.; Yuan, Z. Influence on the methane/air explosion characteristics of the side venting position in a pipeline. *Process Saf. Environ. Prot.* **2017**, *111*, 292–299. [[CrossRef](#)]
14. Pan, C.; Wang, X.; Li, G.; Liu, Y.; Jiang, Y. Influences of a square and circular vent on gasoline vapor explosions and its propagation: Comparative experimental study. *Case Stud. Therm. Eng.* **2021**, *27*, 101225. [[CrossRef](#)]
15. Zhang, C.; Dong, H.; Zhang, K.; Shang, S.; Gao, W. Combined effect of the number and arrangement of multiple vents on the characteristics of vented propane-air mixture explosions in a large L/D ratio duct. *J. Loss Prev. Process Ind.* **2024**, *89*, 105304. [[CrossRef](#)]
16. Zhang, S.; Guo, J.; Yang, F.Q.; Wang, J. Vented deflagration of a hydrogen-air mixture in a rectangular vessel with a hinged aluminum vent panel. *Int. J. Hydrogen Energy* **2019**, *44*, 22733–22739. [[CrossRef](#)]
17. Zhang, Q.; Chen, G.; Huang, X.; Xu, Q.; Ma, J.; Xie, M. Effects of vent layout and vent area on dynamic characteristics of premixed methane-air explosion in a tube with two side-vented ducts. *J. Loss Prev. Process Ind.* **2023**, *83*, 105051. [[CrossRef](#)]
18. Zhou, Y.; Li, Y.; Gao, W. Experimental investigation on unconfined hydrogen explosion with different ignition height. *Int. J. Hydrogen Energy* **2023**, *48*, 20112–20123. [[CrossRef](#)]
19. Qi, B.; Li, H.; Zhai, F.; Yu, M.; Wei, C. Experimental and numerical study on the explosion characteristics of syngas under different venting conditions. *Energy* **2024**, *290*, 130069. [[CrossRef](#)]
20. An, H.; Mu, X. Contributions to Rock Fracture Induced by High Ground Stress in Deep Mining: A Review. *Rock Mech. Rock* **2024**, 1–49. [[CrossRef](#)]
21. Shearer, M.J.; Tam, V.H.Y.; Corr, B. Analysis of results from large scale hydrocarbon gas explosions. *J. Loss Prev. Process Ind.* **2000**, *13*, 167–173. [[CrossRef](#)]
22. Molkov, V.V. Unified correlations for vent sizing of enclosures at atmospheric and elevated pressures. *J. Loss Prev. Process Ind.* **2001**, *14*, 567–574. [[CrossRef](#)]

23. Razus, D.M.; Krause, U. Comparison of empirical and semi-empirical calculation methods for venting of gas explosions. *Fire Saf. J.* **2001**, *36*, 1–23. [[CrossRef](#)]
24. Molkov, V.; Makarov, D.; Puttock, J. The nature and large eddy simulation of coherent deflagrations in a vented enclosure-atmosphere system. *J. Loss Prev. Process Ind.* **2006**, *19*, 121–129. [[CrossRef](#)]
25. Makarov, D.; Verbecke, F.; Molkov, V. Numerical analysis of hydrogen deflagration mitigation by venting through a duct. *J. Loss Prev. Process Ind.* **2007**, *20*, 433–438. [[CrossRef](#)]
26. Bauwens, C.; Chaffee, J.; Dorofeev, S. Experimental and Numerical Study of Methane-air Deflagrations in a Vented Enclosure. *Fire Saf. Sci.* **2008**, *9*, 1043–1054. [[CrossRef](#)]
27. Makarov, D.; Verbecke, F.; Molkov, V.; Kotchourko, A.; Lelyakin, A.; Yanez, J.; Baraldi, D.; Heitsch, M.; Efimenko, A.; Gavrikov, A. An intercomparison of CFD models to predict lean and non-uniform hydrogen mixture explosions. *Int. J. Hydrogen Energy* **2010**, *35*, 5754–5762. [[CrossRef](#)]
28. Li, R.; Malalasekera, W.; Ibrahim, S.; Liu, B. On the mechanism of pressure rise in vented explosions: A numerical study. *Process Saf. Environ. Prot.* **2018**, *117*, 551–564. [[CrossRef](#)]
29. Kodakoglu, F.; Farahani, H.F.; Rangwala, A.S.; Akkerman, V. Dynamics of explosion venting in a compartment with methane-air mixtures. *J. Loss Prev. Process Ind.* **2020**, *67*, 104230. [[CrossRef](#)]
30. Toliás, I.C.; Venetsanos, A.G.; Markatos, N.C.; Kiranoudis, C.T. CFD simulation of hydrogen deflagration in a vented room. *J. Phys. Conf. Ser.* **2015**, *640*, 012036. [[CrossRef](#)]
31. Xing, H.; Qiu, Y.; Sun, S.; Wang, M.; Li, B.; Xie, L. Visualization of explosion characteristics of methane-air mixtures with different ignition positions and vent areas in a large-scale venting chamber. *Fuel* **2020**, *279*, 118380. [[CrossRef](#)]
32. Sun, S.; Wang, M.Y.; Qiu, Y.Y.; Gao, K. Study of flame propagation in an external space under vented explosion conditions. *Energy* **2019**, *178*, 186–194. [[CrossRef](#)]
33. Su, B.; Luo, Z.; Wang, T.; Liu, L. Experimental and numerical evaluations on characteristics of vented methane explosion. *J. Cent. South Univ.* **2020**, *27*, 2382–2393. [[CrossRef](#)]
34. Sun, S.; Qiu, Y.; Xing, H.; Wang, M. Effects of concentration and initial turbulence on the vented explosion characteristics of methane-air mixtures. *Fuel* **2020**, *267*, 117103. [[CrossRef](#)]
35. Wang, Z.; Zhang, Z.; Tian, W.; Wang, Z. Coupling effect of side explosion vent and wire mesh on suppressing methane explosion in a closed duct. *J. Loss Prev. Process Ind.* **2022**, *76*, 104738. [[CrossRef](#)]
36. Chen, D.; Zhang, H.; Li, J.; Liu, K.; Wang, Y.; Huang, Y.; Mao, Z.; Wu, C. A full-scale experimental investigation of natural gas explosion in a 710-m long utility tunnel with multiple pipelines. *Tunn. Undergr. Space Technol.* **2024**, *153*, 106049. [[CrossRef](#)]
37. Ma, Y.; Liang, Z.; Liu, Z.; Zhang, Q.; Zhang, Y. Study on the effect of pre-blended section ratio and hydrogen blended ratio on explosion dynamics of dimethyl ether-hydrogen blended gas. *Combust. Flame* **2024**, *267*, 113600. [[CrossRef](#)]
38. Canu, P.; Rota, R.; Carrà, S.; Morbidelli, M. Vented gas deflagrations a detailed mathematical model tuned on a large set of experimental data. *Combust. Flame* **1990**, *80*, 49–64. [[CrossRef](#)]
39. Mercx, W.P.M. Venting of Gaseous Explosions. *Process Saf. Prog.* **1993**, *12*, 40–46. [[CrossRef](#)]
40. Molkov, V.; Dobashi, R.; Suzuki, M.; Hirano, T. Modeling of vented hydrogen-air deflagrations and correlations for vent sizing. *J. Loss Prev. Process Ind.* **1999**, *12*, 147–156. [[CrossRef](#)]
41. Molkov, V.; Dobashi, R.; Suzuki, M.; Hirano, T. Venting of deflagrations: Hydrocarbon-air and hydrogen-air systems. *J. Loss Prev. Process Ind.* **2000**, *13*, 397–409. [[CrossRef](#)]
42. Bauwens, C.R.; Chaffee, J.; Dorofeev, S.B. Vented explosion overpressures from combustion of hydrogen and hydrocarbon mixtures. *Int. J. Hydrogen Energy* **2011**, *36*, 2329–2336. [[CrossRef](#)]
43. Bauwens, C.R.; Chao, J.; Dorofeev, S.B. Effect of hydrogen concentration on vented explosion overpressures from lean hydrogen-air deflagrations. *Int. J. Hydrogen Energy* **2012**, *37*, 17599–17605. [[CrossRef](#)]
44. Bauwens, C.R.; Dorofeev, S.B. Effect of initial turbulence on vented explosion overpressures from lean hydrogen-air deflagrations. *Int. J. Hydrogen Energy* **2014**, *39*, 20509–20515. [[CrossRef](#)]
45. Tang, P.; Jiang, J. Numerical Simulation of Duct-vented Gas Explosion. *Procedia Eng.* **2011**, *18*, 25–30. [[CrossRef](#)]
46. Qinhuang, L.; Liming, H.; Shuguang, J.; Hao, S. Study on the Numerical Simulation of the Vacuum Cavity Explosion Venting. *Procedia Eng.* **2014**, *84*, 363–368. [[CrossRef](#)]
47. Vermorel, O.; Quillatre, P.; Poinso, T. LES of explosions in venting chamber: A test case for premixed turbulent combustion models. *Combust. Flame* **2017**, *183*, 207–223. [[CrossRef](#)]
48. Wan, S.; Yu, M.; Zheng, K.; Wang, C.; Yuan, Z.; Yang, X. Effect of side vent size on a methane/air explosion in an end-vented duct containing an obstacle. *Exp. Therm. Fluid Sci.* **2019**, *101*, 141–150. [[CrossRef](#)]
49. Zhang, Y.; Jiao, F.; Huang, Q.; Cao, W.; Shi, L.; Zhao, M.; Yu, C.; Nie, B.; Cao, X. Experimental and numerical studies on the closed and vented explosion behaviors of premixed methane-hydrogen/air mixtures. *Appl. Therm. Eng.* **2019**, *159*, 113907. [[CrossRef](#)]
50. Yang, S.; Cai, J.; Yang, Y.; Fang, Q.; Bao, Q.; Wang, S. Investigation of a semi-empirical load model of natural gas explosion in vented spaces. *J. Saf. Sci. Resil.* **2021**, *2*, 157–171. [[CrossRef](#)]
51. Bao, Q.; Fang, Q.; Zhang, Y.; Chen, L.; Yang, S.; Li, Z. Effects of gas concentration and venting pressure on overpressure transients during vented explosion of methane-air mixtures. *Fuel* **2016**, *175*, 40–48. [[CrossRef](#)]
52. Jiang, X.; Fan, B.; Ye, J.; Dong, G. Experimental investigations on the external pressure during venting. *J. Loss Prev. Process Ind.* **2005**, *18*, 21–26. [[CrossRef](#)]

53. Janovsky, B.; Selesovsky, P.; Horkel, J.; Vejsa, L. Vented confined explosion s in Stramberk experimental mine and AutoReaGas simulation. *J. Loss Prev. Process Ind.* **2006**, *19*, 280–287. [[CrossRef](#)]
54. Ferrara, G.; Willacy, S.; Phylaktou, H.; Andrews, G.; Di Benedetto, A.; Salzano, E.; Russo, G. Venting of gas explosion through relief ducts: Interaction between internal and external explosions. *J. Hazard. Mater.* **2008**, *155*, 358–368. [[CrossRef](#)]
55. Proust, C.; Leprette, E. The Dynamics of Vented Gas Explosions. *Process Saf. Prog.* **2010**, *29*, 231–235. [[CrossRef](#)]
56. Zhang, K.; Wang, Z.; Chen, Z.; Jiang, F.; Wang, S. Influential factors of vented explosion position on maximum explosion overpressure of methane-air mixture explosion in single spherical container and linked vessels. *Process Saf. Prog.* **2018**, *37*, 248–255. [[CrossRef](#)]
57. *Fluidyn Ventex Gui User Manual*; Fluidyn: Saint-Denis, France, 2017.
58. Bray, K.N.C.; Libby, P.A.; Moss, J.B. Flamelet Crossing Frequencies and Mean Reaction Rates in Premixed Turbulent Combustion. *Combust. Sci. Technol.* **1984**, *41*, 143–172. [[CrossRef](#)]

Disclaimer/Publisher’s Note: The statements, opinions and data contained in all publications are solely those of the individual author(s) and contributor(s) and not of MDPI and/or the editor(s). MDPI and/or the editor(s) disclaim responsibility for any injury to people or property resulting from any ideas, methods, instructions or products referred to in the content.